Tephra transformations: variable preservation of tephra layers from two well-studied eruptions

Cutler, N.A.[1]; Streeter, R.T.[2], Marple, J.[2], Shotter, L.R.[3], Yeoh, J.S.[3], Dugmore, A.J. [3, 4, 5]

[1] School of Geography, Politics & Sociology, Newcastle University, UK

[2] School of Geography & Sustainable Development, University of St Andrews, UK

[3] School of Geosciences, University of Edinburgh, UK

[4] Department of Anthropology, Washington State University, USA

[5] Graduate Center, City University of New York, USA

Corresponding author:

Nick A Cutler, School of Geography, Politics & Sociology, 5th Floor Claremont Tower, Newcastle University, Newcastle upon Tyne, NE1 7RU, UK

Email: nick.cutler@ncl.ac.uk

Abstract

Volcanologists often use terrestrial tephra layers to reconstruct volcanic eruptions. However, the conversion of fresh tephra deposits into tephra layers is poorly understood. To address this knowledge gap, we surveyed tephra layers emplaced by the 1980 eruption of Mount St Helens, USA (MSH1980) and the 1947 eruption of Hekla, Iceland (H1947). We compared our measurements with observations made shortly after the 1947 and 1980 eruptions, to calibrate the subsequent transformation of the tephra deposit. We expected the tephra layers to retain the broad characteristics of the original deposits, but hypothesized a) changes in thickness and mass loading due to re-working, and b) positive correlations between thickness and vegetation density. We observed some systematic changes in tephra layer properties with distance from the vent and the main plume axis. However, the preservation of the layers varied both between and within our survey locations. Closed coniferous forest appeared to provide good conditions for the preservation of the MSH1980 tephra, as expected; preservation of the H1947 deposit in sparsely vegetated parts of Iceland was much more variable. However, preservation of the MSH1980 deposit in sparsely vegetated areas of eastern Washington State was also excellent, possibly due to biocrust formation. We concluded that the preservation of tephra layers is sensitive to surface conditions at the time of the eruption. These findings have implications for the reconstruction of past eruptions where eruption plumes span regions of variable surface cover.

Key words: Hekla; Mount St Helens; mass loading; biocrusts; kriging; volcanological reconstruction; biophysical feedbacks

Introduction

Layers of tephra preserved in soils are frequently used in the reconstruction of past volcanic eruptions and the evaluation of volcanic hazards (Houghton and Carey 2015). For example, tephra layers may be used to estimate the total volume of pyroclastic material erupted, eruption intensity, column height and the spatial distribution of pyroclastic deposits (Bonadonna and Houghton 2005; Pyle 1989). Inferences based on terrestrial tephra layers have greatly extended the short and rather patchy record of volcanic eruptions based on historical accounts, and made a major contribution to our understanding of volcanism (Lowe 2011). However, they rely on the assumption that the preserved tephra layer is representative of the initial deposit. A great deal can happen to tephra after deposition and the ways in which tephra layers are preserved (or not) are poorly understood (Fig. 1). The formation of tephra layers is difficult to observe directly, as it can be lengthy (unfolding over years to decades) and spatially variable. Furthermore, tephra deposited on land is vulnerable to post-depositional re-working by wind, water and slope processes: in the worst-case scenario, all of the deposited tephra can be lost to erosion (Blong et al. 2017; Pyle 2016). Surface characteristics, notably vegetation cover, can also influence preservation (Cutler et al. 2016a; Cutler et al. 2016b; Dugmore et al. 2018). These factors impose a limit on the information that a tephra layer can provide. Clearly, a deposit that has been extensively re-worked is an unreliable indicator of eruption parameters, but it is often unclear how representative ancient, apparently unmodified, tephra layers are.

[Fig. 1: tephra preservation]

One way to address the knowledge gap surrounding tephra layer preservation is to record the physical characteristics (typically layer thickness, mass per unit area (mass loading), and internal stratigraphy) of a tephra layer and to compare this record with similar measurements made shortly after an eruption. In this way, it should be possible to calibrate the degree of physical transformation that a tephra deposit undergoes during preservation, i.e., the process by which it is incorporated into the sedimentary record over a timescale of decades or longer (it is possible that buried layers may still undergo modification). If the tephra deposit crosses ectones (the transitional regions between distinctive vegetation types, e.g., the boundary between forest and savanna), it should also be possible to investigate the influence of vegetation cover on tephra preservation. To do this, we compared relatively thin (<10 cm) preserved tephra layers from two twentieth century volcanic events – the eruptions of Hekla in 1947 (H1947) and Mount St Helens in 1980 (MSH1980) - with measurements of the tephra deposits taken shortly after the eruptions (i.e., prior to incorporation into the stratigraphic record). Relatively thin tephra layers may be lost in some depositional environments (e.g., due to chemical weathering), but persist in many settings to form an important record of past eruptions.

We expected the tephra layers to capture the overall features of the original deposit. For example, we anticipated that layer thickness and mass loading would, on the whole, decrease with a) distance from the vent and b) distance from the main axis of the eruption plume (Houghton and Carey 2015). With MSH1980 we expected to find an

area of distal secondary thickening described in contemporary reports (Sarna-Wojcicki et al. 1981). However, we also expected transformation of the deposit to varying degrees. We used our results to test two hypotheses:

H1: The preserved tephra layer would be thinner than the initial deposit due to compaction and/or the loss of material due to reworking by wind, water and slope processes; mass/unit area would only be lower due to losses.

H2: Tephra layer thickness would vary according to vegetation cover, with the highest levels of tephra retention (relative to the original deposit) in the areas of densest vegetation (e.g., closed forest) and the lowest in areas of sparse vegetation cover.

Methods

The study areas

We chose the MSH1980 and H1947 tephra layers because the eruptions that produced them were the subject of detailed, contemporaneous studies (refer to Online Resource 1 for details of the historical datasets we used in this study). Both were plinian eruptions that distributed tephra over 1000s of km^2 (Table 1, Figs 2, 3). Crucially, records of initial tephra depth and mass loading, each based on dozens of measurements taken shortly after the eruptions, have been published (Thorarinsson 1954; Waitt and Dzurisin 1981). In the case of MSH1980, some of the researchers who monitored the eruption were still active when we were carrying out the study, and we were able to conduct fieldwork in

collaboration with one of them (Dr Richard Waitt of the USGS). The eruptions are sufficiently recent that vegetation cover in the fallout zones has not changed dramatically (based on photographic evidence). Conversely, the time that has elapsed between the original surveys and our measurements (H1947: 70 years, MSH1980: 35 years) is sufficient to ensure the burial of the layers.

[Table 1: characteristics of the MSH1980 and H1947 eruptions]

We focused our study on areas > 15 km from the vent that received relatively thin initial deposits (~10 cm or less). These areas were spatially extensive and we reasoned that records of the fallout would be numerous and comparatively reliable (as the accurate recording of very thin (sub-mm) and very thick (multiple metre) deposits in the field is challenging: Yang and Bursik 2016). We collected data on tephra thickness and mass loading, two variables used in reconstructions of volcanic eruptions. In the case of the MSH1980 layer, we also recorded the internal stratigraphy in locations within 50 km of the vent. Grain size distribution is another important characteristic of tephra layers. However, a sparsity of tabulated data and major differences between the methodologies and statistics reported in the literature meant it was not possible to make meaningful comparisons between original and recent grain size distributions.

[Fig. 2: Fallout map: MSH1980]

[Fig. 3: Fallout map: H1947]

[Fig. 4: Illustrative photos of the three different environments]

We screened the original datasets and removed the following data points:

- All zero values, because our study focused on $\log_{10}$ thickness and we were not concerned with establishing the edge of the fallout zone;
- Values from locations close to the vent (within a few km), as these are often highly variable, due to partial column collapse and uneven topography (Yang and Bursik 2016);
- Values we judged to be unreliable due to uncertain provenance (H1947 dataset only: refer to Online Resource 1).

This left samples sizes of n = 163 for MSH1980 and n= 62 for H1947.

Clearly, there is likely to be a small degree of uncertainty in the measurements themselves: Engwell et al. (2013) estimated observational error in the measurement of centimeter-scale tephra layers at ~10%; similar estimates have been made by others (Bonadonna et al. 2015). However, the estimated error varies according to tephra thickness and it is difficult to quantify this uncertainty for historical measurements made by several different people under varying conditions. Given the relatively small observational error described in the literature, we have assumed that the historical measurements in the literature are accurate to the nearest mm for the purposes of this study.

Interpolation of initial tephra thickness

Ideally, the location of our measurements would have *exactly* replicated those used in the original surveys, as recent research has demonstrated that tephra layers can be highly variable over small spatial scales (Cutler et al. 2016b). Unfortunately, this was not possible for the following reasons:

a) The original survey locations were not permanently marked. We had coordinates for the MSH1980 sample points, but not H1947.
b) Many of the original measurements came from substrates that do not preserve tephra layers (e.g., road surfaces, the roofs of cars and buildings, etc.)
c) Some of the original locations no longer exist (including measurements made on ships that passed under the H1947 eruption plume, or sites subsequently destroyed by anthropogenic activity and/or geomorphological processes).
d) Some deposits occurred on heavily managed landscapes, including ploughed fields (eastern Washington State), and field systems dedicated to grazing/fodder production where tephra was removed manually (southern Iceland).

Terrestrial tephra layers are prone to disturbance, and these kinds of problems will face any researcher seeking to compare extant tephra layers with measurements made shortly after the eruption.

Given the near impossibility of replicating survey locations exactly, we had to take measurements as close as possible to the original coordinates and use interpolation techniques to estimate initial deposit thicknesses in our sample locations (due to the

relative sparsity of mass loading data, we decided not to interpolate this property). Many previous studies have attempted to interpolate tephra thickness from a few points, usually during the drafting of isopach maps. Our goal was slightly different: we wanted to interpolate initial tephra thickness (with known variance) at arbitrary locations downwind from the eruption. This goal meant we were not concerned with many of the issues that have preoccupied previous researchers, such as calculating the total volume of the deposit or inferring the edge of the fallout zone (Burden et al. 2013; Engwell et al. 2015; Yang and Bursik 2016).

Initial tephra thicknesses in our sampling locations were estimated from contemporary records using the method developed by Yang & Bursik (2016). Briefly, this statistical approach assumes that tephra thickness at an arbitrary location comprises: 1) a trend component and 2) a random local component. Hence, when the data are log-transformed, tephra thickness may be expressed as:

$$Th(s) = T(s) + Res(s) \quad \text{[eqn 1]}$$

where $Th(s)$ is the thickness at location s, $T(s)$ is the trend thickness and $Res(s)$ the local, or residual, variation. The only data required to interpolate deposit thickness in the model are a) the dominant wind direction during the eruption and b) some known values of tephra thickness (in this case, the original values).

198 The trend component is largely a function of distance from the source vent and the
199 prevailing wind at the time of the eruption (which is assumed to be stable in strength
200 and direction). The local component is the result of numerous, small-scale processes
201 (e.g., turbulence structures in the plume) and is assumed to be spatially stochastic.
202 Yang and Bursik's (2016) approach models the two components separately and can
203 therefore accommodate phenomena such as the secondary thickening of the MSH1980
204 deposit observed by Sarna-Wojcicki *et al*. (1981). Following Yang and Bursik (2016), we
205 modelled the trend component using standard regression techniques, using radial
206 distance ($R(s)$) and downwind distance ($Dd(s)$) as explanatory variables (Online
207 Resource 2).
208
209 The local component was modelled using ordinary kriging on the residuals from the
210 multiple regression model. Kriging is an established interpolation technique that
211 provides a minimum variance estimate of a value at unmeasured locations, using a
212 model of autocorrelation structure (the theoretical variogram). Detailed descriptions of
213 kriging are available elsewhere (e.g., Isaaks and Srivastava 1989). Briefly, we produced
214 sample variograms from the residuals of the linear (trend) model. The sample
215 variograms described the relationship between semi-variance (a measure of
216 autocorrelation) in $\log_{10}(Th)$ and the distance between sampled locations. The sample
217 variograms were fitted with commonly used mathematical models by a process of trial-
218 and-error, using the 'gstat' package running in R (Pebesma 2004). We fitted spherical,
219 exponential and Gaussian models and selected the best fit by means of visual
220 inspection and a comparison of the weighted sum of squared errors for each model

(Bivand et al. 2013). The theoretical variogram that resulted was used during kriging, carried out using the 'gstat' package after checking the residuals for normality.

Yang and Bursik's (2016) approach necessarily presents a much-simplified version of reality: it is unable to accommodate factors such as changes in wind direction or eruption dynamics, and complex processes in the atmosphere are reduced to simple distance relationships. However, it does provide a robust, pragmatic and conceptually straightforward method of inferring parameters such as tephra thickness at unmeasured locations. It is particularly useful when details of eruption parameters are unavailable.

Field sampling of extant tephra layers

MSH1980

We conducted our surveys in the Gifford Pinchot National Forest (GPNF), 15 – 50 km from Mt St Helens (hereafter, proximal locations), and at distal locations close to Ritzville, WA (approx. 300 km from the eruption source: Fig. 2) in August 2015. We chose sampling locations where the initial deposit thickness was moderate (~5 - 10 cm), i.e., places where the tephra-fall would not have obliterated vegetation. The two sampling areas have different climates: the GPNF has a moist, temperate climate; in contrast, the Ritzville location has an arid, continental climate and frequently experiences high winds (Online Resource 3). The vegetation cover in the two locations also varies. The proximal location (~15 – 50 km from the vent) was characterized by closed coniferous forest, composed primarily of hemlock (*Tsuga* sp.) and Douglas fir

(*Pseudotsuga menziesii*) (Fig. 4a). We surveyed old growth forest sites where the trees on the sampling locations would have been mature at the time of the 1980 eruption. The distal location was characterized by shrub/grassland dominated by sagebrush (*Artemisia* sp.), a vegetation type known as sagebrush steppe (Fig. 4b). The sagebrush locations we sampled had patchy vegetation cover: the areas between sagebrush/grass patches often lacked vascular plants. Instead, these apparently bare areas were covered by a thin (< 2.5 cm) biological soil crust (biocrust) composed of mosses, lichens and, presumably, microorganisms such as fungi and cyanobacteria (Johansen 1993).

In the GPNF, we surveyed tephra layers along two transects established in 1980 (designated B-B' and C-C' in Waitt & Dzurisin (1981): see Fig. 2b). The transects ran approximately north-south, perpendicular to the main axis of the 18 May eruption plume. We surveyed 20 locations in total. The mean separation distance between our locations and the original samples was 1.5 ± 0.4 km, with the majority of locations (10 of the 18 we used in our analysis) < 1 km from the 1980 survey locations. We recorded a) total tephra layer thickness; b) the thickness of each unit within the tephra layer (where it was possible to distinguish such features) following the nomenclature outlined in Waitt and Dzurisin (1981) (refer to Online Resource 1 for details); c) the characteristics of the understory vegetation cover and d) the thickness of soil/litter cover. We also collected tephra samples from nine locations (refer to Online Resource 4). We used loss on ignition (LOI) analysis to establish the proportion of organic material in the tephra layer. The samples were homogenized before removing representative sub-samples. The

sub-samples were dried at 105 °C for a minimum of eight hours, then heated to 550 °C for four hours to drive off organic material.

In the sagebrush steppe vegetation around Ritzville, we identified seven sampling locations on an east-west transect (Fig. 2c). The survey of tephra layer thickness was similar to that implemented in the GPNF (Online Resource 4). We collected a tephra sample from one of the sampling locations, using the same methods deployed in the GPNF, and backfilled the excavations.

H1947

We carried out surveys of the H1947 layer in southern Iceland in August 2017. We targeted areas that were a) close to Thorarinsson's original (1954) sampling points (mean separation distance 0.3 ± 0.1 km) and b) in the zone where the original tephra deposit was of moderate thickness (< 10 cm). The region has a cold, moist maritime climate and experiences frequent frosts (Online Resource 3). Our sampling locations varied in character and the original points were imprecisely located, so we applied case-by-case reasoning to locate suitable survey areas (refer to Online Resource 4 for details of our approach). We sampled 12 locations in total.

Results

Interpolation of original tephra thickness

Our analysis of the original thickness measurements showed that both layers exhibited exponential thinning with distance. The most parsimonious trend models were linear in all cases; as the linear models were effective for our purposes (i.e., interpolating tephra thickness 10s of km from the vent) we did not explore more complex non-linear models. The introduction of breaks of slope can improve estimates of overall fallout volume, because they capture variations in thickness close to the vent (Bonadonna and Houghton 2005). However, this refinement was not relevant to our models, as the slope for the whole deposit adequately captures the variation at the scale of interest. As the plots of $\log_{10}$(thickness) vs absolute and downwind distance provided no compelling evidence for introducing breaks in the trend models (Online Resource 5), we applied multiple linear regression to model the trend in tephra thickness for both tephra layers. The regressions were highly significant (MSH1980: $F_{2,160} = 116.2$, $p < 0.001$; H1947: $F_{2,59} = 45.7$, $p < 0.001$), with adjusted R^2 values of ~0.6 in both cases.

The residuals of the trend models were approximately normal and therefore suitable for ordinary kriging. The experimental variograms exhibited predictable increases in semivariance with distance and we fitted spherical models to these variograms to characterize local variations in tephra thickness (Online Resources 6, 7).

Field surveys

The MSH1980 tephra layer was found in all the sampling locations we visited in the GPNF and in many cases the deposits could be divided into distinct stratigraphic sub-units based on grain size and/or colour. The tephra layers were close to the surface:

most were covered by a thin (1 – 5 cm) layer of organic material (Figs 5, 6a). The contacts between the tephra and the layers above and below were generally sharp. In many sections, decayed timber (presumably from the 1980 forest floor) was clearly visible at the base of the tephra deposit. Based on visual inspection, the stratigraphies within each of the sample layers were consistent with the descriptions in Waitt & Dzurisin's (1981) study. Within-site variability, expressed as a coefficient of variation (CV; i.e., the sample standard deviation at each sampling location divided by the sample mean) ranged from 0 – 33%, with most locations having a CV between 10 and 25% (Table 2). There was a thick layer of re-worked tephra in GP03 and this data point was omitted from our analysis. Stratigraphic Unit B was missing (or not spotted) in GP04. LOI analysis indicated that the tephra samples from the GPNF contained an appreciable quantity of organic material/moisture (mean = 10.8 ± 1%).

Tephra layers were also found in all of the locations we selected around Ritzville. In undisturbed areas, the MSH1980 tephra layer was found just below a thin (3 – 25 mm) biocrust. The layer was uniformly fine and pale grey (Fig. 6b). In most cases, both the top and bottom surfaces of the layer were sharply defined. Within-site variability was generally low: although a CV figure of 33% was observed at R06, the remaining six locations had values below 16% (Table 2). LOI analysis of a single sample from the Ritzville area indicated that the proportion of organic material/moisture was 7.7%.

Areas with an intact H1947 layer were hard to locate. We eventually identified 12 locations that satisfied our criteria (Fig. 3, Table 2). All but one of the sampling locations

was within 500 m of Thorarinsson's (assumed) original measurement; the greatest separation distance was 1.16 km. The H1947 layer was more variable than MSH1980 in terms of thickness: the CV figures ranged from 21-65%, with most of our sampling locations displaying a CV around 30% (Table 2). The layer was also buried more deeply, with ~4 – 10 cm of overlying sediment (Fig. 6c), and appeared to be unstratified. LOI analysis indicated that the H1947 tephra samples had consistently low organic content (0.4 – 3.9%; mean = 2.3 ± 0.4%).

[Table 2: Summary of tephra measurements]

[Fig. 5: MSH1980 stratigraphy]

Tephra layer thickness and mass loading

In the GPNF, tephra thickness varied predictably along transect C-C', i.e., the values were lowest toward the margins of the fallout zone (where the layer became increasingly patchy) and thickest towards the axis of the eruption plume (Fig. 5). The layer was thicker along transect B-B', but did not exhibit a systematic thickening towards the axis of the fallout zone. Mass loadings for the GPNF sampling locations ranged from 1.6-10.3 g cm^{-2} (Fig. 7). The highest mass loading was recorded close to the main axis of the eruption plume (i.e., where Waitt & Dzurisin's transect AA' intersects CC': Fig. 7b). Mass loadings decreased with distance from the plume axis. There was no systematic variation in layer thickness along the east-west transect line established outside Ritzville (within an area of secondary thickening). The tephra sample taken from this location had a mass loading of 2.3 g cm^{-2} (Fig. 7a).

[Fig. 6: Field images of tephra layers]

[Fig. 7: MSH mass loadings]

The thickness and mass loading of the H1947 layer did not vary predictably with distance from the vent and main axis of the plume. The most distal sampling location (Hk12) had the thinnest tephra layer (1.5 cm). However, the layer was a similar thickness (1.9 cm) at the most proximal sampling location (Hk01) (Table 2). The sampling location with the thickest layer (Hk08: 5.9 cm) was an intermediate distance from the vent, and away from the main axis of the plume. Most sampling locations had a thickness of 2 -3 cm, regardless of location. The mass loading figures were similarly unpredictable, with most sampling locations between 2 – 3 g cm^{-2} (Table 2). Sampling location Hk08 was an outlier: the mass loading here (4.2 g cm^{-2}) was the highest recorded and twice that of adjacent locations.

[Fig. 8: Hekla mass loading results]

Comparison of findings with original measurements

Thickness measurements from the MSH1980 layer were positively correlated with interpolated initial thicknesses (Fig. 9). However, there was a difference between the GPNF and Ritzville samples. The Ritzville measurements were close to, or slightly below, the interpolated values (Fig. 9a, blue points). The tephra layer here had a mean thickness of 3.4 ± 0.2 cm. An initial thickness of 4.2 cm was recorded at a nearby

location in 1980 (IAVCEI 2010), i.e., the thickness of the preserved layer was around 80% of the initial deposit. In contrast, the layer in the GPNF appeared to be *thicker* than the interpolated values (Fig. 9a, red points), in some cases by up to 200% (GP01). Our measurements fell below the interpolated values on just two sampling locations.

The mass loading data from MSH1980 followed a similar pattern. Transect CC' (along which we collected our GPNF mass loading samples) is about 32 km from MSH, measured along the plume axis. Reading from a plot of mass loading vs distance in Sarna-Wojcicki *et al*. (1981: their figure 339), the estimated mass loading at the intersection of the plume axis with CC' was 8 g cm^{-2}. We recorded a figure of 10.3 g cm^{-2} for approximately the same location (i.e., slightly higher than the original figure). The samples from Ritzville told a similar story. The isomass map in Sarna-Wojcicki *et al*. (their figure 338) suggests mass loadings between 2.0 and 2.5 g cm^{-2} around Ritzville. Our recorded value of 2.3 g cm^{-2} fitted neatly in this range.

The correlation between initial and preserved thickness was much weaker for the H1947 layer (Fig. 9b). The measured thicknesses were consistently lower than the interpolated initial values (10 of the 12 sampling locations). In many cases, the preserved layer was >50% thinner than the initial deposit. The pattern of the mass loading values was similar: most were much lower than those observed in 1947 (Fig. 8). Two locations departed from this: the mass loading at Hk08 was similar to the initial value; the value recorded for Hk05 (2.7 g cm^{-2}) greatly exceeded Thorarinsson's measurement (0.9 g cm^{-2}).

404

405 [Fig. 9: Comparison of measured and interpolated values]

406

407

408 **Discussion**

409 The preservation of the tephra layers varied both within and between the two eruptions.
410 Preservation of the MSH1980 layer in areas of light anthropogenic disturbance was
411 good. Broad trends in thickness and mass loading apparent in the initial deposit were
412 retained in the tephra layer (i.e., both metrics decreased with distance from the vent and
413 the main axis of the plume). This was particularly clear on transect C-C' (the sampling
414 locations on B-B' were probably too close to the plume axis to show a marked pattern).
415 Small-scale stratigraphy was also preserved (GPNF sampling location) and within-site
416 variability was low: small- (metre-) scale factors had not obscured the volcanic signal.
417 The same could not be said of the H1947 layer, which exhibited considerable variability
418 at all scales and disrupted stratigraphy.

419

420 We anticipated that the tephra layers would undergo a degree of post-depositional
421 transformation, particularly the H1947 layer (deposited on a snow-covered, managed
422 landscape). A degree of bioturbation would be expected in moist, productive habitats
423 like the GPNF (Blong et al. 2017). Even if no tephra were lost through the action of wind
424 and water, thinning due to compaction is likely. Very little research has been conducted
425 on the rate/magnitude of tephra compaction. Some researchers have applied 'rule of
426 thumb' adjustments to allow for compaction: for example, Sarna-Wojcicki *et al*. (1981)

increased their estimate of initial layer thickness in the Ritzville area by a factor of two after a rainfall event, based on mass loading figures. Placing constraints on the rate of tephra compaction, either by direct measurement of fresh deposits, or experimental manipulation, would clearly be a useful goal for future research.

Given these factors, the level of preservation we observed in the MSH1980 layer was unexpected. Our surveys revealed little or no evidence of bioturbation. We did not find litter in the samples during collection, average organic content (in the form of fine roots, soil organic matter (SOM) and soil microbes) was comparatively low and contacts with the surrounding soil were usually sharp. These observations are consistent with limited mixing, and, whilst it is probable that some tephra grains have been lost to other soil horizons, the thickness and mass loading figures suggest such losses were limited. Major re-working of the layer by slope processes was only observed in one sampling location in the GPNF (GP03, subsequently omitted from our analysis).

Our previous work in Iceland suggests that biophysical feedbacks, specifically vegetation structure (and its likely impact on surface wind conditions), plays an important role in tephra retention (Cutler et al. 2016a; Cutler et al. 2016b; Dugmore et al. 2018). Closed forest (such as that found in the GPNF) should, in principle, be a good environment for the stabilization of tephra, because the forest canopy reduces surface wind speed (Online Resource 3) and intercepts a significant proportion of the precipitation. The degree of ground disturbance by large herbivores is also limited, when compared to pasture land. The coniferous forests of the Pacific North West are

highly productive, and the rapid accumulation of an organic layer on top of the tephra could assist in preservation, as could the formation/persistence of a thick ground layer of vegetation.

Even allowing for favourable conditions, the fact that most of the GPNF measurements exceeded the interpolated initial thicknesses is a puzzle. The apparent discrepancy could be due to the input of allochthonous (non-volcanogenic) sediment post-deposition. We assumed that the inorganic component of the samples was mainly tephra, but it is possible that a small component of fine, non-volcanogenic sediment (i.e., produced by rock weathering) may have been included (particularly in the samples from the semi-arid sagebrush steppe), compensating for losses of tephra. However, the fine-scale stratigraphy of the layers suggests that additions of this type were limited. Uncertainty in the interpolation process might have also contributed towards the seemingly anomalous result. The trend model included unexplained variance; furthermore, we were not able to replicate the original sampling locations and kriging variance increases with distance from the points used to generate the sample variogram (Bivand et al. 2013). However, we believe the pattern observed in the GPNF was real because:

a) It was persistent (all but one of our measurements exceeded the interpolated values, sometimes by a factor of two);

b) The trend model was effective in explaining variance in tephra depth; local variance made a relatively minor contribution to tephra thickness (typically < 20% in the case of the GPNF measurements);

c) None of our GPNF sampling locations were more than 7.4 km from a USGS survey location (typically much closer), so the kriging variance was low (Online Resource 7);

d) Where our sampling locations were close to the 1980 sites (< 1 km separation, in some instances) the pattern was preserved (i.e., it is unlikely to be an artefact of the interpolation).

In addition, the mass loading figure for GP16, close to the main axis of the plume, exceeded the value estimated Sarna-Wojcicki *et al*.'s (1981) survey.

If the tephra layer in the GPNF is, indeed, thicker and heavier than the deposit measured shortly after the eruption, this suggests a) rapid and near-complete stabilization of the tephra, with little compaction and b) the addition of further tephra after first measurements were made. Further tephra may have been added to the 1980 layer after the 18 May eruption, as there were subsequent tephra-producing eruptions. The plume from one of these eruptions (22 July) was blown eastwards and may have added a few millimetres of tephra to the 18 May deposit (Waitt et al. 1981). Furthermore, it is possible that tephra from the 18 May eruption was deposited *after* measurement. Zobel and Antos (1991) noted that coniferous trees trapped tephra during the initial air-fall event, and that this material reached the ground sometime after the eruption. Measurement techniques may also account for some apparent discrepancies. Sarna-Wojcicki *et al*. (1981) noted that other observers reported greater thicknesses of tephra, but suggested that these reports were due to earlier observations (i.e., they were made before compaction had occurred) or the reporting of maximum,

rather than average, thicknesses. The incorporation of organic material (typically around 11% by mass in GPNF) may also have enhanced the thickness of the layer. Whatever the reasons, it seems that preservation of the tephra layer under close coniferous forest has been unusually good.

We observed very little site-to-site variation in the thickness of the distal MSH1980 layer. This was unsurprising as the sampling locations lie parallel with the main axis of the plume in a region where the rate of change in thickness with distance was low. As in the GPNF, the degree of tephra retention on undisturbed land around Ritzville was remarkable, particularly given how susceptible this fine-grained material must have been to erosion by wind (Online Resource 3). In order to retain so much fine material, stabilization of the tephra must have been rapid, particularly as the patchy vegetation of the sagebrush steppe would seem to be a much less favourable environment for preservation than the closed canopy forest. The retention of the tephra layer in open areas (i.e. between sagebrush/grass patches) was particularly surprising, as the ground surface was relatively smooth and exposed to the elements. The lack of variation in tephra thickness between vegetated and non-vegetated areas around Ritzville was also unexpected. In Iceland, the thickness of tephra layers is positively correlated with vegetation height/density (Cutler et al. 2016a), so we expected that the layer would be thicker under sagebrush clumps.

The lack of variation in the Ritzville locations implies that the mechanisms for stabilizing tephra in open areas were just as effective as those operating beneath vegetation.

Again, it is possible that biophysical processes have influenced tephra preservation: we suspect that the stabilization of tephra in open areas was due to biocrust formation. A thin crust was present in all the locations we sampled and was clearly capable of capping-off the underlying deposit. Cyanobacteria can colonize suitable substrates in a matter of days to initiate biocrust formation. Thereafter, biological succession can occur, with increasing cover of bryophytes and lichens being particularly important. Rozenstein *et al*. (2014) note that in certain conditions a biocrust can form within weeks, and that biocrust formation on fine substrates is much faster, and more homogeneous, than it is on coarse grains. An investigation of the biocrust composition and rate of formation would be a useful focus of future study.

In contrast to the MSH1980 layer, preservation of the H1947 layer was spatially variable, even in areas where presumed human interference was low. The mass loading observed at Hk08, which initially appeared to be an outlier, was actually closest to the 1947 value. This area differs from the other sampling locations, in that it sits in the bottom of a shallow, semi-enclosed basin. It is therefore possible that tephra re-mobilized from adjacent, unvegetated slopes supplemented the initial deposit. Most other sampling locations had experienced losses of tephra, but one (Hk05) appeared to have gained material. Southern Iceland is a wet and windy locality (Online Resource 3) subject to significant cryoturbation (evidenced by patterned ground and frost hummocks (*thufur*), on our field sites). Vegetation is low-growing and often sparse. However, we know that tephra from recent eruptions in southern Iceland has been extensively mobilized in the months following the eruption, even when the eruption was in spring

(Arnalds et al. 2013). Similar remobilization has been observed following other eruptions, both in Iceland (Liu et al. 2014) and South America (Panebianco et al. 2017; Wilson et al. 2011). During the 1947 eruption, the surface vegetation would have been suffering from winter dieback. It is therefore likely that a significant proportion of the initial H1947 deposit was re-mobilized after its initial deposition. Fine-scale variation in surface roughness would have led to the local differences in tephra thickness and mass loading that we observed. For example, on Hk11 we noted that the H1947 layer was absent from the 'crests' of small hummocks. Furthermore, the tephra fell during winter when there was patchy snow cover and extensive ground ice formation. Tephra falling on snow patches would have been re-worked when the snow melted. Any remaining stratigraphy would have been disrupted by the formation of ground (needle) ice. Geomorphological processes have clearly been important in the preservation of the H1947 layer. In this setting, accurate reconstruction of the fallout from the preserved layer would be extremely challenging. Had the tephra fallen on equivalent vegetation in a less geomorphologically active setting, the preservation of the layer might have been much better.

Tephrostratigraphy relies on the use of isochronous layers, which, ideally, represent only the primary fallout. However, we suspect that terrestrial tephra deposits are routinely transformed by processes operating over a range of (frequently overlapping) timescales. The operation of these processes may make it hard to separate unmodified and transformed deposits reliably. When tephra is exposed at the surface, it is subject to both erosion and the stabilizing effect of vegetation. Compaction and disruption by ice

growth and decay can occur both above and below ground. Once interred, it is affected by both biological and abiotic processes such as root growth, bioturbation, through-flow and solifluction. Some transformations, such as those resulting from earthquakes and land sliding, may occur through the full depth of the soil/regolith. We do not know the duration of the processes that physically transform tephra layers; they may operate for as long as the tephra layer exists. We suspect that the rate of change is highest just after deposition and decreases with time as the tephra layer is progressively buried. Transformation of the tephra may be continuous or episodic; the rate of change may alter abruptly as different factors come into play (e.g., the rate of transformation could reduce sharply on first burial as the tephra is no longer affected by surface processes). We suspect that the genesis of terrestrial tephra layers varies on a site-by-site basis according to climate, vegetation cover, topographic location, time and the properties of both the soil/regolith and the tephra layer itself. However, the trajectory of change can only be established by longitudinal studies. Regardless of how the transformation proceeds, it appears that terrestrial tephra deposits can undergo modification without showing obvious signs of re-working (e.g., diffuse contacts with the soil, disrupted stratigraphy, etc.) and this process can operate without markedly increasing spatial patchiness (i.e., all of the deposit in a given area can be transformed in the same way). Indeed, our experience with the H1947 layer suggests that tephra layers can become more spatially homogeneous over time. Hence, terrestrial tephra layers have to be carefully assessed for transformations before they are used to infer volcanological parameters and processes.

Conclusions

We hypothesized that the MSH1980 and H1947 tephra layers would capture the overall characteristics of the fallout that created them (i.e., systematic thinning and reduction in mass loading). However, we expected the transformation of both their physical properties and internal structure (H1). We also anticipated that vegetation cover would mediate this transformation, e.g., the degree of preservation of the MSH1980 layer in GPNF would be higher than that in the sagebrush steppe (H2). We found that the MSH1980 tephra layer captured the overall characteristics of the original deposit. However, the degree of preservation varied markedly between Washington State and Iceland – the MSH1980 layer had a higher level of preservation - and the layers did *not* thin predictably during preservation. It was difficult to calibrate the preservation of the MSH1980 layer in the GPNF, because there is strong evidence that contemporary measurements underestimated the original deposit. If the original measurements had captured the whole deposit, we may well have seen the thinning/mass loss we anticipated. In Iceland, the H1947 layer did not retain the overall characteristics of the initial deposit, due to the operation of local-scale biophysical feedbacks which resulted in variable preservation. The collection of more samples, spread over a wider area, might have given a clearer picture, but it was clear that the signal from the initial deposit was largely scrambled. Hence, the support for our first hypothesis was qualified, at best.

It appeared that vegetation cover played a role in tephra preservation. The Icelandic sampling locations, characterized by low-growing and sometimes sparse vegetation,

had variable (often poor) preservation. In contrast, the closed tree cover of the GPNF was associated with a high level of tephra preservation. However, against expectations, we also found good preservation in the sparse vegetation of the sagebrush steppe, hinting at the previously unsuspected significance of biocrusts (a cover type characteristic of ~70% by area of global drylands: Ferrenberg et al. 2015). Hence, whilst we found evidence consistent with H2, we also revealed a more nuanced relationship between ground cover, geomorphological processes and tephra preservation. These findings reinforce our belief that reconstructions of past eruption histories based on terrestrial tephra records are sensitive to surface conditions (specifically vegetation cover) at the time of the eruption. Hence, inferred volcanological parameters based on these deposits should be treated with due caution. The effect of surface conditions on tephra preservation (and, by extension, volcanological inferences) will be particularly marked when a tephra deposit crosses regions of contrasting vegetation cover.

Acknowledgements

We thank Kathy Cashman and two anonymous reviewers for their helpful comments. Financial support was provided by the National Science Foundation of America through grant 1202692 ‘Comparative Island Ecodynamics in the North Atlantic’, and grant 1249313 ‘Tephra layers and early warning signals for critical transitions’ (both to AJD). We are also grateful to Icelandic landowners for access, Ben Fitzhugh and Tim Kohler for fieldwork support, and Richard Waitt (USGS) for his advice, particular regarding the selection of field sites and the interpretation of the MSH1980 tephra layer.

633

634

635 **References**

636

637 Arnalds O, Thorarinsdottir EF, Thorsson J, Dagsson Waldhauserova P, Agustsdottir AM
638 (2013) An extreme wind erosion event of the fresh Eyjafjallajokull 2010 volcanic ash. Sci
639 Rep-UK 3
640 Bivand RS, Prebesma E, Gómez-Rubio V (2013) Applied spatial data analysis with R.
641 Springer, New York
642 Blong R, Enright N, Grasso P (2017) Preservation of thin tephra. Journal of Applied
643 Volcanology 6. https://doi.org/10.1186/s13617-017-0059-4
644 Bonadonna C, Biass S, Costa A (2015) Physical characterization of explosive volcanic
645 eruptions based on tephra deposits: Propagation of uncertainties and sensitivity
646 analysis. Journal of Volcanology and Geothermal Research 296:80-100
647 Bonadonna C, Houghton BF (2005) Total grain-size distribution and volume of tephra-
648 fall deposits. B Volcanol 67:441-456
649 Burden RE, Chen L, Phillips JC (2013) A statistical method for determining the volume
650 of volcanic fall deposits. B Volcanol 75
651 Cutler NA, Bailey RM, Hickson KT, Streeter RT, Dugmore AJ (2016a) Vegetation
652 structure influences the retention of airfall tephra in a sub-Arctic landscape. Prog Phys
653 Geog 40:661-675

654 Cutler NA, Shears OM, Streeter RT, Dugmore AJ (2016b) Impact of small-scale
655 vegetation structure on tephra layer preservation. Sci Rep-UK 6.
656 https://doi.org/10.1038/srep37260
657 Dugmore A, Streeter R, Cutler N (2018) The role of vegetation cover and slope angle in
658 tephra layer preservation and implications for Quaternary tephrostratigraphy.
659 Palaeogeogr Palaeocl 489:105-116
660 Engwell SL, Aspinall WP, Sparks RSJ (2015) An objective method for the production of
661 isopach maps and implications for the estimation of tephra deposit volumes and their
662 uncertainties. B Volcanol 77. https://doi.org/10.1007/s00445-015-0942-y
663 Engwell SL, Sparks RSJ, Aspinall WP (2013) Quantifying uncertainties in the
664 measurement of tephra fall thickness. Journal of Applied Volcanology 2. 10.1186/2191-
665 5040-2-5
666 Ferrenberg S, Reed SC, Belnap J (2015) Climate change and physical disturbance
667 cause similar community shifts in biological soil crusts. PNAS 112:12116-12121
668 Houghton B, Carey RJ (2015) Pyroclastic fall deposits. In: Siggurdsson H, Houghton B,
669 McNutt SR, Rymer H, Stix J (eds) Encyclopdia of Volcanoes. Academic Press, London,
670 pp 599-616
671 IAVCEI (2010) Data sets. IAVCEI Commission on Tephra Hazard Modelling.
672 http://www.ct.ingv.it/iavcei/data/MSH/MSH80_location-thickness.txt. Accessed 25 April
673 2018
674 Isaaks EH, Srivastava RM (1989) An introduction to applied geostatistics. Oxford
675 University Press, New York

676 Johansen JR (1993) Cryptogamic crusts of semiarid and arid lands of North America. J
677 Phycol 29:140-147
678 Liu EJ, Cashman KV, Beckett FM, Witham CS, Leadbetter SJ, Hort MC, Guomundsson
679 S (2014) Ash mists and brown snow: Remobilization of volcanic ash from recent
680 Icelandic eruptions. Journal of Geophysical Research-Atmospheres 119:9463-9480
681 Lowe DJ (2011) Tephrochronology and its application: A review. Quat Geochronol
682 6:107-153
683 Panebianco JE, Mendez MJ, Buschiazzo DE, Bran D, Gaitan JJ (2017) Dynamics of
684 volcanic ash remobilisation by wind through the Patagonian steppe after the eruption of
685 Cordon Caulle, 2011. Sci Rep-UK 7
686 Pebesma EJ (2004) Multivariable geostatistics in S: the gstat package. Comput Geosci
687 30
688 Pyle DM (1989) The thickness, volume and grainsize of tephra fall deposits. B Volcanol
689 51:1-15
690 Pyle DM (2016) Field observations of tephra fallout. In: Mackie S, Cashman K, Ricketts
691 H, Rust A, Watson M (eds) Volcanic Ash. Elsevier, Amsterdam, pp 25-38
692 Rozenstein O, Zaady E, Katra I, Karnieli A, Adamowski J, Yizhaq H (2014) The effect of
693 sand grain size on the development of cyanobacterial biocrusts. Aeolian Res 15:217-
694 226
695 Sarna-Wojcicki AM, Shipley S, Waitt RB, Dzurisin D, Wood SH (1981) Areal distribution,
696 thickness, mass, volume, and grain size of air-fall ash from the six major eruptions in
697 1980. In: Lipman PW, Mullineaux DR (eds) The 1980 eruption of Mount St Helens,
698 Washington, U.S. U.S. Department of the Interior, USGS, Washington D.C., pp 577-600

699 Thorarinsson S (1954) The tephra fall from Hekla on March 29th 1947. Societas
700 Scientarium Islandica, Reykjavik
701 Waitt RB, Dzurisin D (1981) Proximal air-fall deposits from the May 18 eruption -
702 stratigraphy and field sedimentology. In: Lipman PW, Mullineaux DR (eds) The 1980
703 eruption of Mount St. Helens, Washington. US Department of the Interior, USGS,
704 Washington D.C., pp 601-616
705 Waitt RB, Hansen VL, Sarna-Wojcicki AM, Wood SH (1981) Proximal air-fall deposits of
706 eruptions between May 24 and August 7, 1980 - stratigraphy and field sedimentology.
707 In: Lipman PW, Mullineaux DR (eds) The 1980 eruption of Mount St. Helens,
708 Washington. U.S. Department of the Interior, USGS, Washington D.C., pp 617-628
709 Wilson TM, Cole JW, Stewart C, Cronin SJ, Johnston DM (2011) Ash storms: impacts of
710 wind-remobilised volcanic ash on rural communities and agriculture following the 1991
711 Hudson eruption, southern Patagonia, Chile. B Volcanol 73:223-239
712 Yang QY, Bursik M (2016) A new interpolation method to model thickness, isopachs,
713 extent, and volume of tephra fall deposits. B Volcanol 78.
714 https://doi.org/10.1007/s00445-016-1061-0
715 Zobel DB, Antos JA (1991) 1980 tephra from Mount St Helens - spatial and temporal
716 variation beneath forest canopies. Biol Fert Soils 12:60-66
717
718

Table captions

Table 1 Characteristics of the MSH1980 and H1947 eruptions; the estimated fallout area from MSH1980 is based on the area of the 1 mm isopach given in Engwell *et al*. (2015)

Table 2 Summary of survey data (T = thickness; CV = coefficient of variation in thickness measurement; SE = standard error). Site codes: GP = Gifford Pinchot National Forest; R = Ritzville; Hk = Hekla

728 **Figure captions**

729

730 **Fig. 1** Conceptual diagram illustrating the post-depositional transformation of tephra
731 layers

732

733 **Fig. 2** MSH1980 sampling locations; our sampling points are indicated by the numbered
734 red circles; the original sampling points are indicated with open circles and the isopachs
735 of 1980 fallout with orange lines; the State boundary is shown with a continuous black
736 line; a) location plan, showing the proximal (GPNF) and distal (Ritzville) sampling areas;
737 the location of Mount St Helens is indicated by a black triangle; b) detail of the GPNF
738 sample locations; the blue lines indicate transects established in the original survey of
739 the tephra deposit; black parallel lines indicate major roads; c) detail of the Ritzville
740 sample locations (the location of Ritzville is indicated by a black square). Isopachs and
741 sampling points from Sarna-Wojcicki *et al*. (1981); tephra thicknesses are in mm

742

743 **Fig. 3** H1947 sampling locations (red circles), with the original sample locations
744 indicated by open circles; isopachs (orange lines) from Thorarinsson (1954);
745 settlements are indicated by black square; icecaps are outlined in black; tephra
746 thicknesses are in mm

747

748 **Fig. 4** The three different environments that we surveyed; a) the closed coniferous
749 forest that characterizes the GPNF sample locations (for scale, the trees in the middle

ground are approximately 50 cm in diameter); b) sagebrush steppe around Ritzville; c) heathland in southern Iceland (note the eroded slopes in the middle ground)

Fig. 5 The average thickness of the MSH1980 layer in the GPNF (sampling location reference numbers are given below each section). Data from our sampling locations have been arranged along Waitt & Dzurisin's B-B' and C-C' section lines and the designation of the tephra units follows their nomenclature (Waitt and Dzurisin 1981). The position of section A-A' (which approximates the main axis of the plume) is shown in each case

Fig. 6 Representative images of the tephra layers showing a) the MSH1980 layer in the GPNF; b) the MSH1980 layer at a distal location outside Ritzville and c) the H1947 layer. Note the more recent Eyjafjalajökull 2010 tephra layer above the H1947 deposit, and the older Katla 1918 layer below

Fig. 7 MSH1980 mass loading data; a) Waitt and Dzurisin's (1981) mass loading data, showing their isomass lines (blue, with mass in g cm^{-2}) and our sampling locations (red circles); our observed mass loading for the Ritzille area is in bold red text; b) our mass loading figures for the GPNF sampling locations (in g cm^{-2}), compared to the isomass lines from the original survey; Waitt and Dzurisin's transect lines are shown for reference; c) our mass loading figures arranged along Waitt and Dzurisin's (1981) transect C-C' in the GPNF; the red vertical line indicates the intersection with transect A-A', which coincides with the plume axis

Fig. 8 H1947 mass loading data; Thorarinsson's (1954) original measurements are shown as green circles, scaled according to his measurements (the green figures in g cm^{-2}); our measurements represented by red circles on the same scale (the red figures, also in g cm^{-2}); the orange line indicates Thorarinsson's 1 mm isopach line; open circles indicate Thorarinsson's original sampling points and black squares settlements; icecaps are outlined in black

Fig. 9 Comparison of measured and interpolated values from MSH1980 (top) and H1947 (bottom)

Figure 1

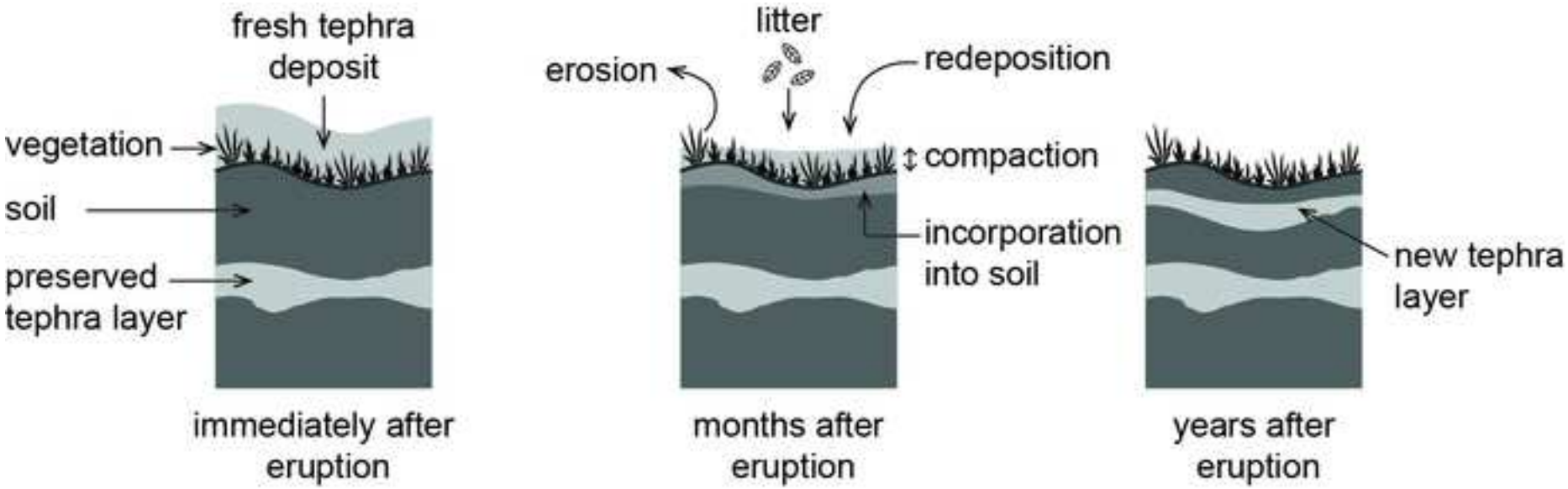

Figure 2

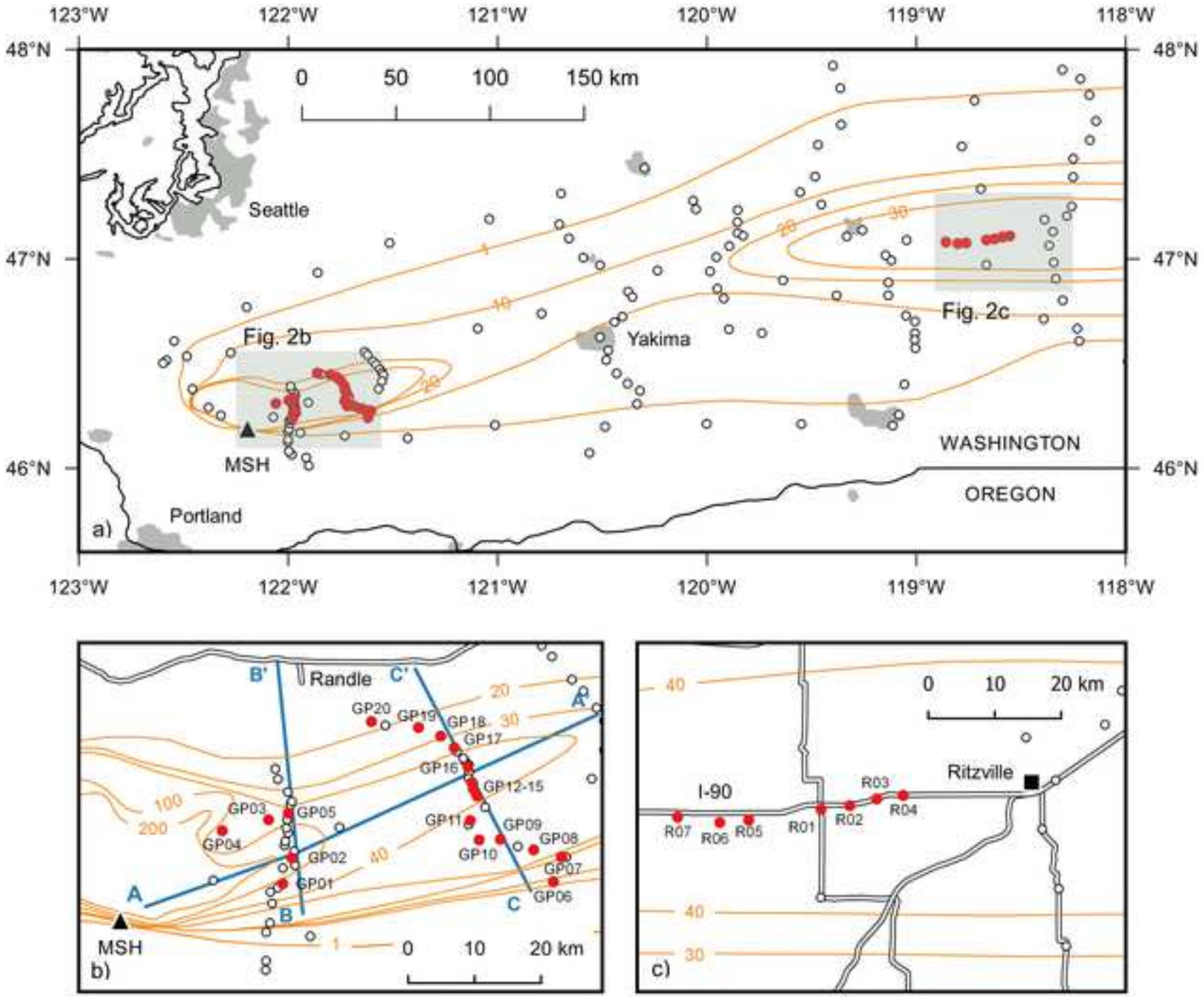

Figure 3

Click here to access/download;Figure;Fig. 3_H1947_map.jpg

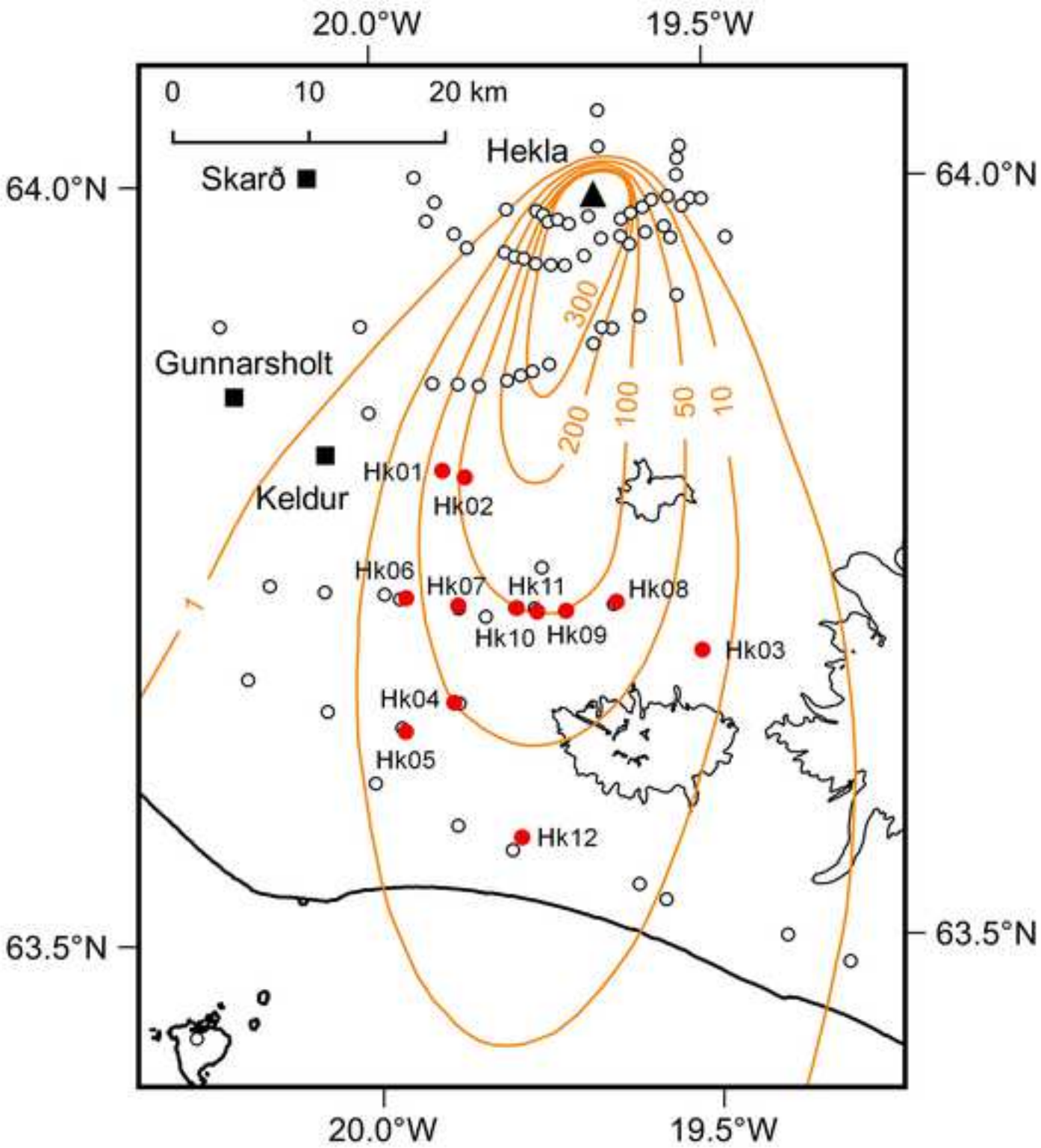

Figure 4

Figure 5

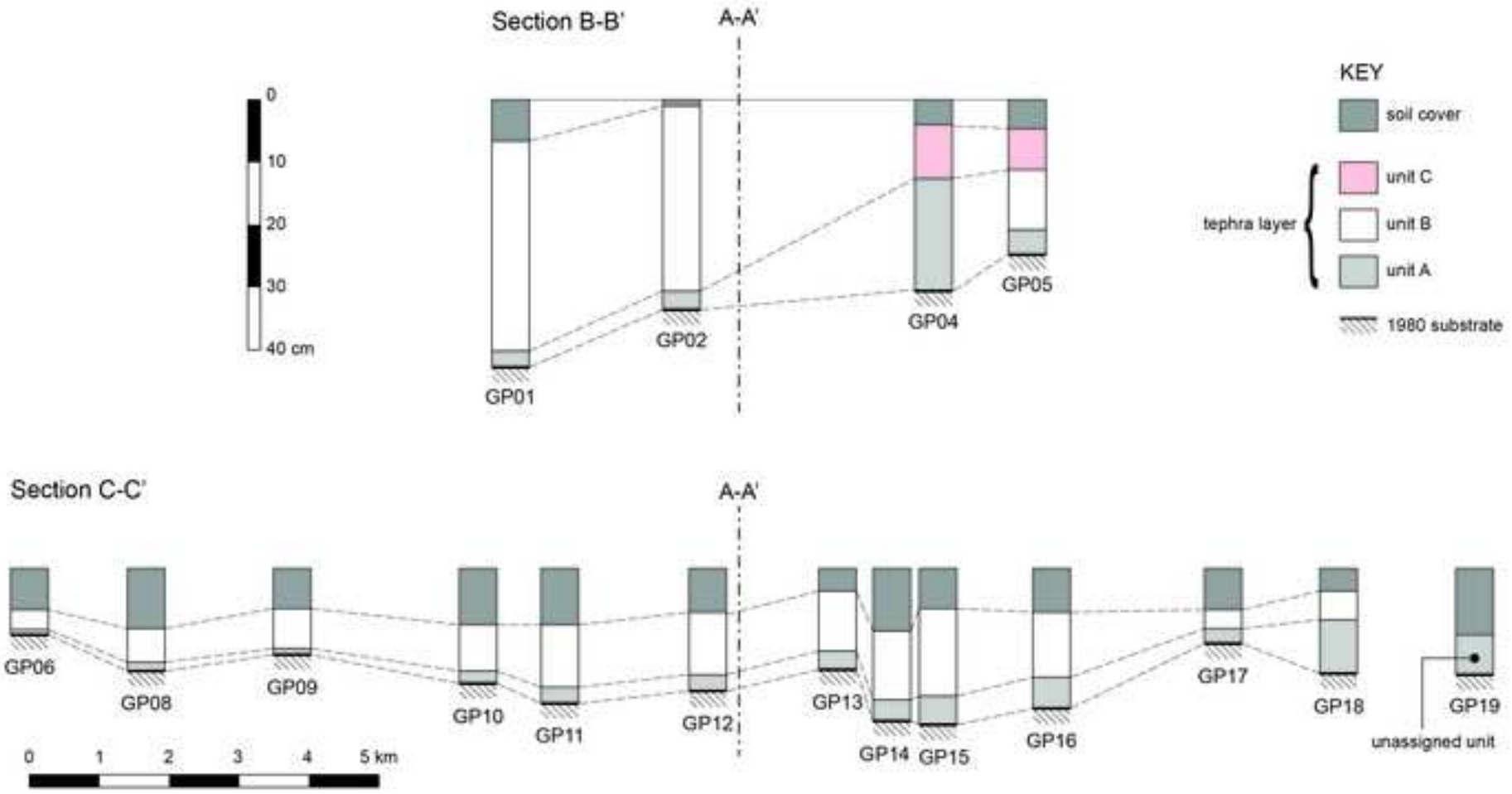

Figure 6

Click here to access/download;Figure;Fig. 6_Tephra images.jpg

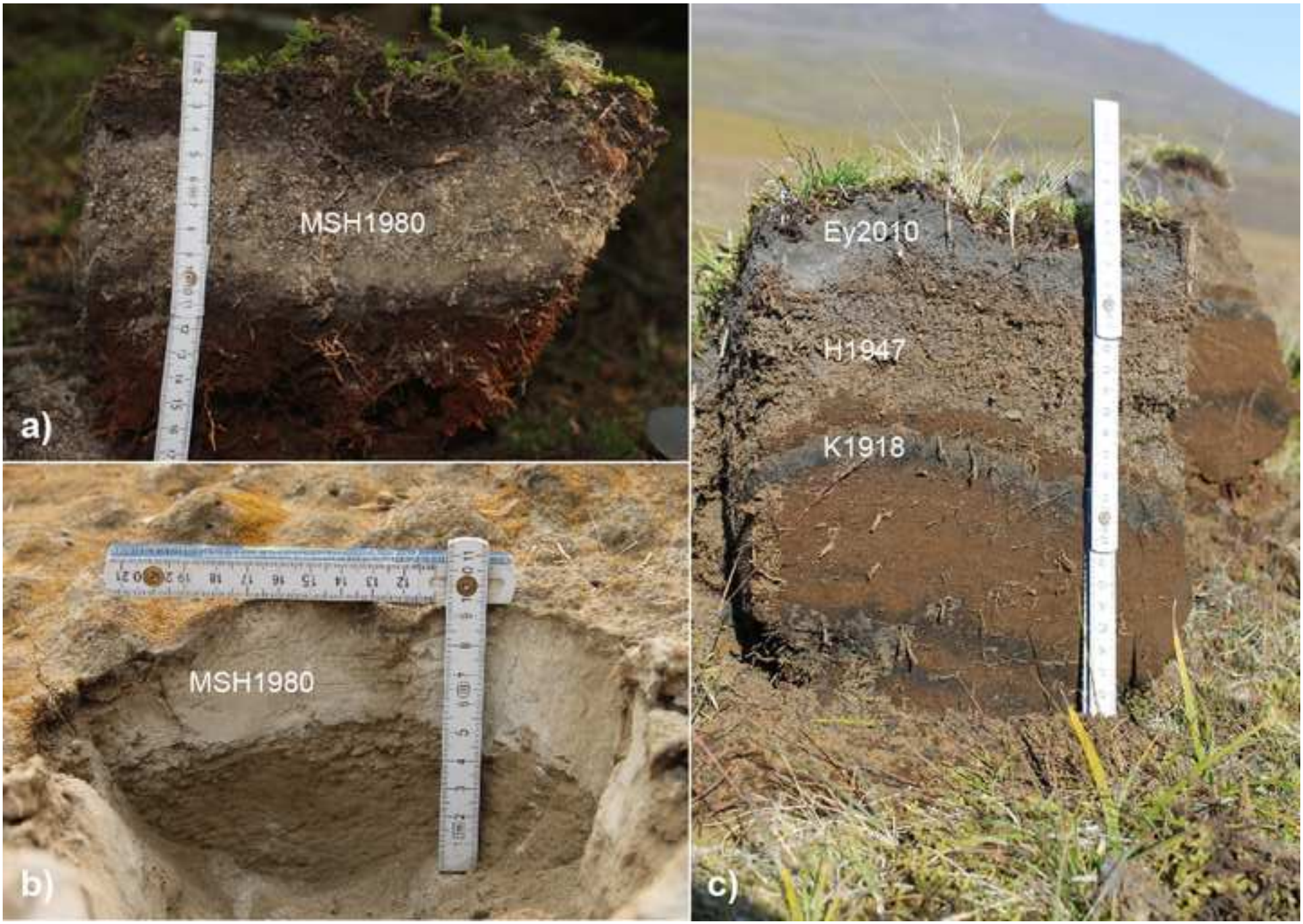

Figure 7

Click here to access/download;Figure;Fig. 7_MSH_ML_rev1.jpg

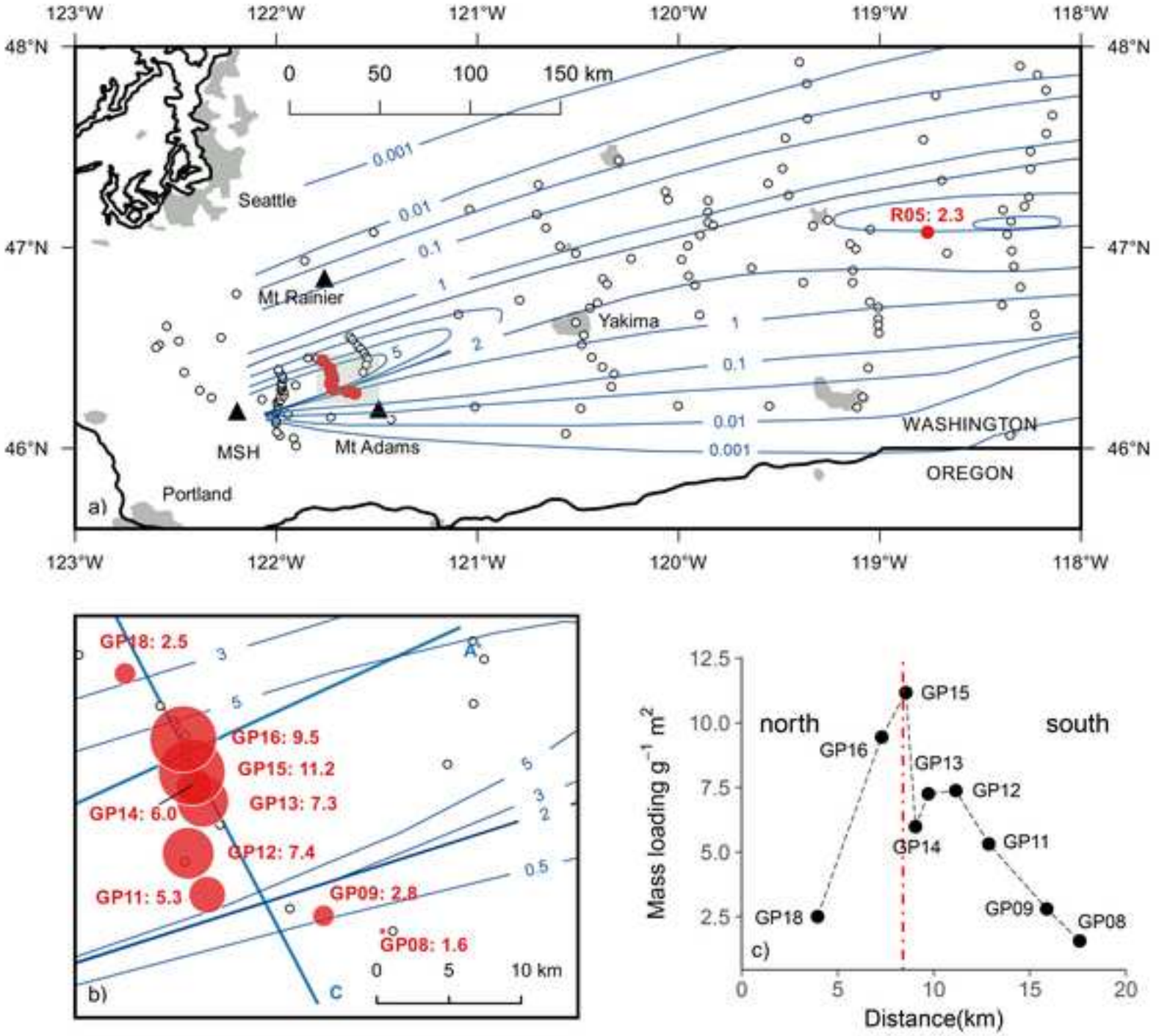

Figure 8

Click here to access/download;Figure;Fig. 8_Hekla_ML_rev1.jpg

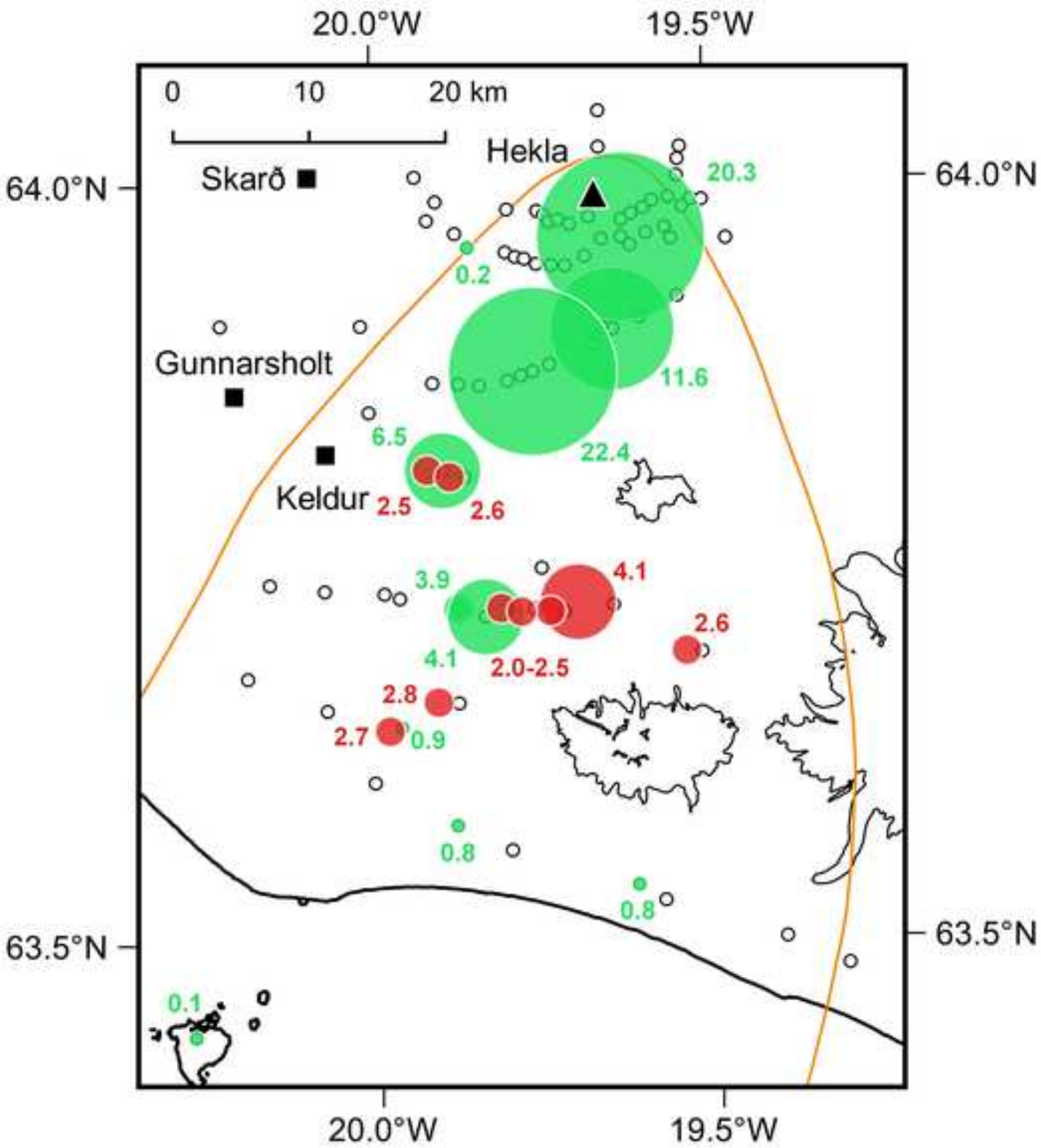

Figure 9

Click here to access/download;Figure;Fig. 9_Interpolated T vs measured T.jpg

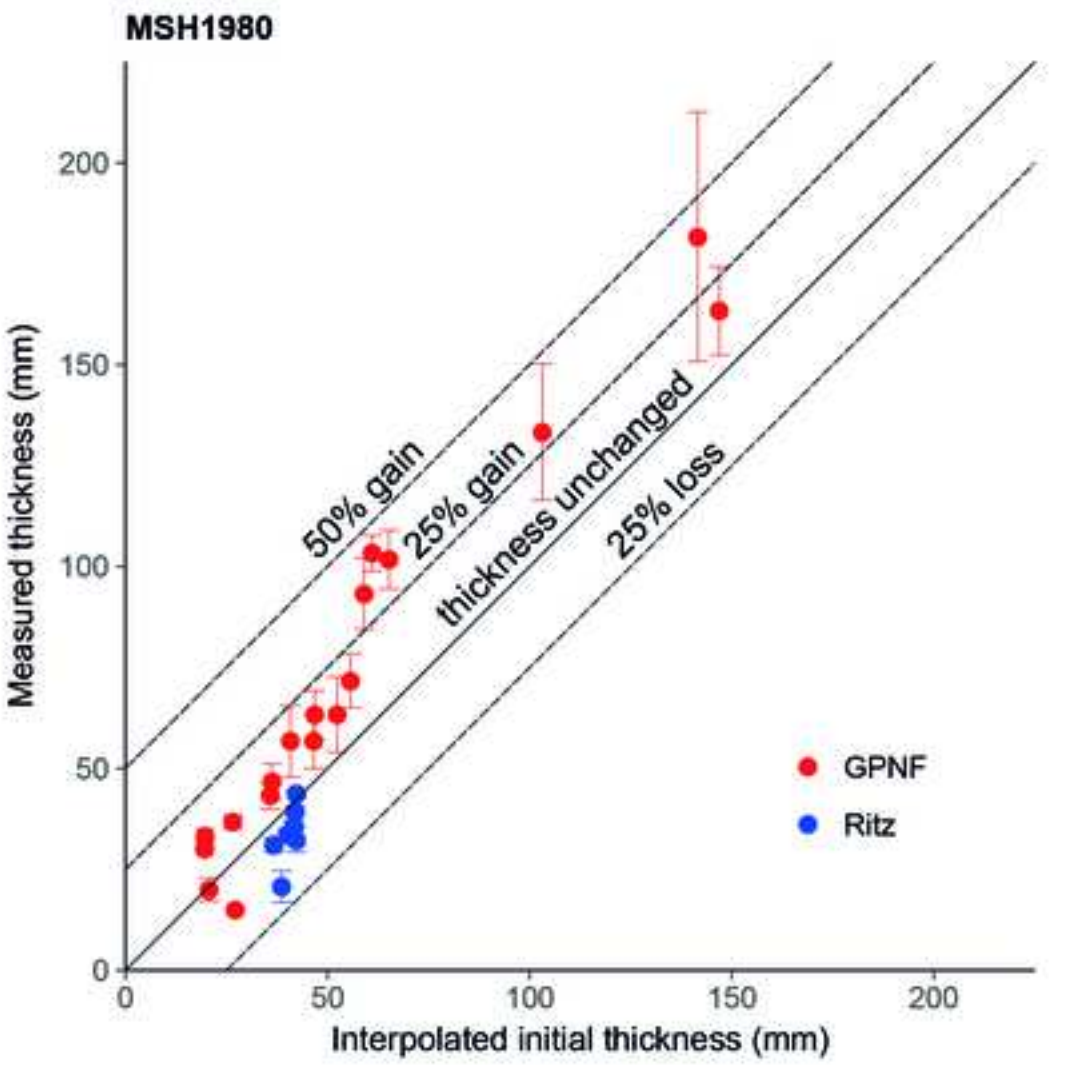

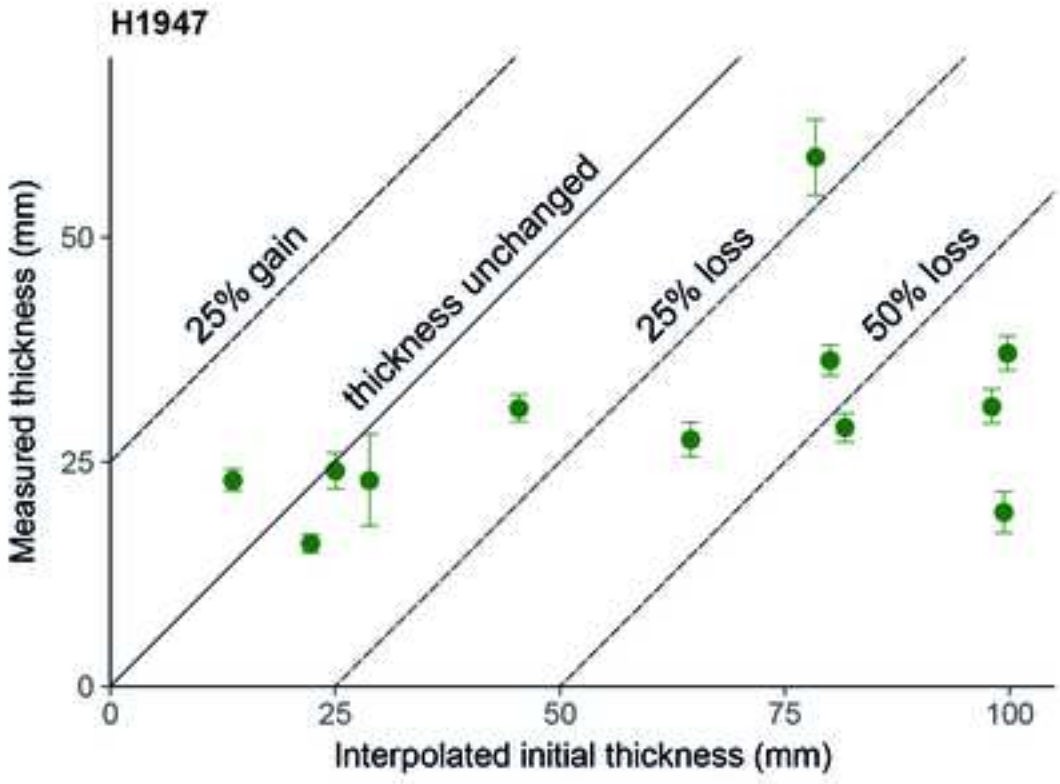

Eruption	Date	VEI	Tephra vol. (km^3 DRE)	Area of fallout (km^2)	Thickness half distance (km)	Main source
Hekla 1947 (H1947)	29 March 1947	4	0.045	3130	21.2	Thorarinsson (1954)
Mt St Helens1980 (MSH1980)	18 May 1980	5	0.250	~140,000	34.4	Sarna-Wojcicki *et al*. (1981)

Table 1

	Site ID	WGS84 °N	WGS84 °E	distance from vent (km)	mean thickness, T (mm)	T SE (±, mm)	CV in thickness (%)	mass loading (g cm^{-2})
MSH1980	GP01	46.23954	-121.97872	17.5	181.7	30.9	29	NA
	GP02	46.27365	-121.96663	19.8	163.3	10.9	12	NA
	GP04	46.30986	-122.05902	16.8	133.3	16.9	22	NA
	GP05	46.33316	-121.97138	23.3	101.7	7.3	12	NA
	GP06	46.24216	-121.61931	44.7	20.0	2.9	25	NA
	GP07	46.27471	-121.60789	46.2	30.0	0.0	0	NA
	GP08	46.27495	-121.60868	46.1	33.3	1.7	9	1.6
	GP09	46.28448	-121.64542	43.6	36.7	1.7	8	2.8
	GP10	46.29844	-121.68956	40.7	46.7	4.4	16	NA
	GP11	46.29767	-121.71782	38.6	56.7	8.8	27	5.3
	GP12	46.32348	-121.72968	38.7	63.3	6.0	16	7.4
	GP13	46.35586	-121.72059	40.8	63.3	9.3	25	7.3
	GP14	46.36508	-121.72563	41.0	71.7	6.7	16	6.0
	GP15	46.37405	-121.72748	41.3	93.3	8.8	16	11.2
	GP16	46.39465	-121.73271	42.1	103.3	4.4	7	9.5
	GP17	46.42008	-121.75088	42.6	56.7	6.7	20	NA
	GP18	46.43559	-121.76901	42.5	43.3	3.3	13	2.5
	GP19	46.44701	-121.79836	41.7	15.0	0.0	0	NA
	GP20	46.45489	-121.86100	39.0	13.3	4.4	57	NA
	R01	47.09090	-118.66449	288.2	32.3	3.0	16	NA
	R02	47.09590	-118.62557	291.2	43.7	0.9	3	NA
	R03	47.10487	-118.58917	294.1	39.3	1.2	5	NA
	R04	47.10965	-118.55353	296.8	35.7	1.2	6	NA
	R05	47.07618	-118.76224	280.6	33.7	1.2	6	2.3
	R06	47.07300	-118.80140	277.7	20.7	3.9	33	NA
	R07	47.08041	-118.85823	273.9	31.0	1.7	10	NA
H1947	Hk01	61.81116	-19.89899	21.5	19.4	2.3	44	2.5
	Hk02	63.80656	-19.86562	21.3	36.3	1.7	21	2.6
	Hk03	63.68988	-19.51749	33.9	24.0	2.0	37	2.6
	Hk04	63.65824	-19.88710	37.3	31.0	1.5	22	2.8
	Hk05	63.63962	-19.95975	40.4	23.0	1.2	23	2.7
	Hk06	63.72763	-19.95592	31.1	23.0	5.1	65	NA
	Hk07	63.72218	-19.87866	30.4	27.5	1.9	35	NA
	Hk08	63.72272	-19.64339	29.6	58.9	4.2	35	4.1
	Hk09	63.71741	-19.71861	29.6	37.1	1.9	25	2.0
	Hk10	63.71984	-19.79180	29.7	28.8	1.6	28	2.5
	Hk11	63.71721	-19.76161	29.8	31.2	1.9	27	2.1
	Hk12	63.56869	-19.79022	46.4	15.9	1.0	30	NA

Table 2

ESM1

ESM2

Click here to access/download

Supplementary Material

ESM_2_rev.pdf

ESM3

Click here to access/download

Supplementary Material

ESM_3_rev.pdf

ESM4

ESM5

ESM6

ESM7